MDPI

Article

Magnetohydrodynamic and Ferrohydrodynamic Fluid Flow Using the Finite Volume Method

Grigorios Chrimatopoulos [1,†]**, Efstratios E. Tzirtzilakis** [2,†] **and Michalis A. Xenos** [1,*,†]

1 Department of Mathematics, University of Ioannina, 45110 Ioannina, Greece; grigorisxrimas3@gmail.com
2 Fluid Mechanics and Turbomachinery Laboratory, Department of Mechanical Engineering, University of the Peloponnese, 26334 Patras, Greece; etzirtzilakis@uop.gr
* Correspondence: mxenos@uoi.gr
† These authors contributed equally to this work.

Abstract: Many problems in fluid mechanics describe the change in the flow under the effect of electromagnetic forces. The present study explores the behaviour of an electric conducting, Newtonian fluid flow applying the magnetohydrodynamics (MHD) and ferrohydrodynamics (FHD) principles. The physical problems for such flows are formulated by the Navier–Stokes equations with the conservation of mass and energy equations, which constitute a coupled non-linear system of partial differential equations subject to analogous boundary conditions. The numerical solution of such physical problems is not a trivial task due to the electromagnetic forces which may cause severe disturbances in the flow field. In the present study, a numerical algorithm based on a finite volume method is developed for the solution of such problems. The basic characteristics of the method are, the set of equations is solved using a simultaneous direct approach, the discretization is achieved using the finite volume method, and the solution is attained solving an implicit non-linear system of algebraic equations with intense source terms created by the non-uniform magnetic field. For the validation of the overall algorithm, comparisons are made with previously published results concerning MHD and FHD flows. The advantages of the proposed methodology are that it is direct and the governing equations are not manipulated like other methods such as the stream function vorticity formulation. Moreover, it is relatively easily extended for the study of three-dimensional problems. This study examines the Hartmann flow and the fluid flow with FHD principles, that formulate MHD and FHD flows, respectively. The major component of the Hartmann flow is the Hartmann number, which increases in value the stronger the Lorentz forces are, thus the fluid decelerates. In the case of FHD fluid flow, the major finding is the creation of vortices close to the external magnetic field source, and the stronger the magnetic field of the source, the larger the vortices are.

Keywords: ferrohydrodynamics; magnetohydrodynamics; biomagnetic fluid dynamics; finite volume method

1. Introduction

For many years, there has been an enormous amount of research concerning various biomedical applications of magnetic flows, i.e., magnetohydrodynamics (MHD) [1,2] and ferrohydrodynamics (FHD) [3,4]. A relatively new area of research combining the principles of MHD and FHD is biomagnetic fluid dynamics (BFD). According to this formulation a magnetic fluid can exhibit both polarization and electrical conductivity. From this perspective, the forces that are exerted on the fluid are those arising from the magnetization due to the polarization of the fluid and the Lorentz force due to the interaction of the magnetic field with the electric current formed by the fluid flow. One of the most characteristic natural fluids, possessing both properties of polarization and electrical conductivity, is blood, and there are many recent studies considering the BFD formulation and general

biomedical applications of magnetic flows [5,6]. Such applications include certain cancer treatments which require clean separation of the white cells from the whole blood for the chemical treatment. Red blood cells, when oxygenated, have the characteristics of a diamagnetic fluid, which makes them prone to a magnetic field. The blood is collected in a device with a surrounding magnetic field which separates the red blood cells. To achieve faster results, the magnetic susceptibility of the red blood cells is increased using magnetic microspheres that are bound to them [7]. The measurement of blood inside a vessel can be a difficult process. Due to the diamagnetic characteristics of blood, when a magnetic field is applied, a potential gradient is generated and can be measured by sensors inside the walls. Utilizing this technique, the blood flow can be measured without contaminating the blood inside [8].

A study presented in [9] depicts the application of a magnetic field on a biomagnetic fluid such as blood, with a similar magnetic field scheme. In that study, the authors examine the thermal radiation using the stream function vorticity, a well-known method for solving the governing equations of fluid flows. A key factor that is studied is the change in the viscosity, which is assumed to be an exponential function of temperature. This has a more realistic meaning since the temperature affects the fluid viscosity. Several applications of the magnetic field on a biomagnetic fluid are also present. The numerical results depicted show the creation of vortices near the magnetic field source. The numerical results have been compared with experimental and commercial software data, indicating a close relation. The thermal radiation affects the recirculation of the fluid, as it reduces the vortices created by the magnetic field.

Especially for the FHD and BFD physical problems, the polarization terms in the governing equations constitute very dense source terms that finally result in the formation of vortices in the flow field. These source terms can also generate numerical instabilities and divergence of the overall algorithm. Moreover, many BFD applications involve the use of artificially created nanoparticles, which dramatically increase the magnetization force. As a result, biofluids can behave like ferrofluids and very high values of the ferromagnetic number can be attained. Since the ferromagnetic number expresses somehow the ratio of the magnetization to the viscous forces, when the Reynolds number decreases, for a given magnetic field strength, the magnetic number is drastically increased. For some very high values of the magnetic number, some numerical techniques may fail to converge. Another factor which increases the difficulty of applying classical methods is the necessary manipulations of the governing equations in order to assure the diagonal dominance of the matrix of the unknowns or to attain convergence for very high magnetic numbers [10].

Studies that examine ferromagnetic fluid flows with various numerical techniques such as the fourth-order Runge–Kutta and Runge–Kutta–Fehlberg 45 methods can be found in [11,12], respectively. In these studies, the authors investigate the fluid flow over the boundary layer of a Jeffery fluid in a porous medium over a shrinking/stretching sheet with the application of a magnetic field and the fluid flow of a ferromagnetic nanofluid over a stretching sheet with the effect of a magnetic dipole. In [13], the shooting method is used for the investigation of different hybrid nanofluids and ferrofluids. Results have been also published utilizing analytical solutions with various techniques such as the similarity method along with the homotopy method [14], as well as the form of hypergeometric functions also with the similarity method [15]. In these studies, the effects of the magnetic field are presented along with heat transfer and radiation.

Among the numerical methodologies widely used for the solution of several BFD problems are various algorithms involving discretization using the finite element method (FEM). FEM using spatial discretization and an unconditionally stable backward finite difference scheme for the time integration was used in [16,17]. The FEM method was also used in [18,19], whereas algorithms involving control-based volume FEM [20], both FEM and the dual reciprocity boundary element method [21], and least squares FEM [22] have also been used. Finally, similar or more complex BFD problems have been solved using COMSOL [23] and a meshless point collocation method (MPCM) along with the moving

least squares (MLS) approximation [24,25]. The aforementioned studies indicate that there is an ongoing interest for the implementation of numerical algorithms suitable for the solution of BFD flow problems.

The physical properties, assumptions, and mechanism of the reaction of the applied magnetic field have also been stated and investigated in numerous variations of BFD Hartmann fluid flow problems. Thus, in the present study, the main effort is focused on the implementation of a numerical algorithm also suitable for BFD flow problems. The basic characteristics of the present algorithm are (i) the set of equations is solved using a simultaneous direct approach; (ii) the discretization is achieved using the finite volume method (FVM); and (iii) the solution is attained solving an implicit non-linear system of algebraic equations.

The advantage of using this technique is that using FVM it is quite easy to implement a variety of boundary conditions in a non-invasive manner, since the unknown variables are evaluated at the centroids of the volume elements and not at the boundary faces [26]. Moreover, the numerical solution is obtained using a direct approach, which creates more robust results since the governing equations are subject to minimum manipulations in contrast to other classical techniques like the stream function vorticity formulation, also used for the solution of BFD problems [10].

The two basic configurations of magnetic Hartmann fluid flow problems are studied in the present paper. The first one is that of MHD Hartmann flow, where an external magnetic field is vertically applied to the channel. For this case an analytical solution can be found, introducing a test problem, where the analytical solution can be compared with the numerical one. The second configuration is the FHD flow, where the applied magnetic field is spatially varying. Comparisons for this case are more difficult to perform and the validation of the results is made qualitatively through results documented in previously published papers.

In the simultaneous approach which is used here, all equations compose a single system of equations which is discretized using FVM. This approach on a very fine grid can be very time consuming and expensive in terms of memory when the system is non-linear and tightly coupled. On the other hand, the solution is obtained using a direct approach, which creates more robust results since the manipulations of the governing equations of each problem are minimal. Finally, due to this implicit direct approach, accurate solutions can be obtained using relatively sparse grids. This study examines the Hartmann flow and the fluid flow with FHD principles that formulate MHD and FHD flows, respectively. The major component of the Hartmann flow is the Hartmann number, where a larger value corresponds to stronger Lorentz forces, which cause deceleration in the fluid. In the case of FHD fluid flow, the major finding is the creation of vortices close to the external magnetic field source, and the stronger the magnetic field of the source, the larger the vortices are.

2. Mathematical Formulation

2.1. Hartmann Flow

The Hartmann flow studies the flow of an electrically conducting fluid while a magnetic field is vertically applied to the bottom channel wall. It also studies the disturbance of the magnetic field due to the electrically conducting fluid. This flow configuration (Hartmann flow) can be considered as a special and simplified magnetohydrodynamic (MHD) case.

The equations that formulate the Hartmann flow at first are the x-momentum of the Navier–Stokes equations and the x-component of the induction equation, as shown below:

$$\rho\left(u\frac{\partial u}{\partial x} + v\frac{\partial u}{\partial y}\right) = -\frac{\partial p}{\partial x} + \mu\left(\frac{\partial^2 u}{\partial x^2} + \frac{\partial^2 u}{\partial y^2}\right) - uB_y^2 + vB_xB_y,$$

$$u\frac{\partial B_x}{\partial y} + v\frac{\partial B_x}{\partial y} = \frac{1}{\mu\sigma}\left(\frac{\partial^2 B_x}{\partial x^2} + \frac{\partial^2 B_x}{\partial y^2}\right) + B_x\frac{\partial u}{\partial x} + B_y\frac{\partial u}{\partial y},$$

(1)

where μ is the fluid viscosity and σ is the electrical conductivity of the fluid. Using the following non-dimensional terms:

$$\bar{q}' = \frac{\bar{q}}{u_0}, \quad \bar{\nabla}' = L\bar{\nabla}, \quad p' = \frac{p}{\rho\, u_0^2}, \quad \bar{B}' = \frac{\bar{B}}{B_0} \tag{2}$$

the system of equations in (1) takes the following form:

$$u'\frac{\partial u'}{\partial x'} + v'\frac{\partial u'}{\partial y'} = -\frac{\partial p'}{\partial x'} + \frac{1}{Re}\left(\frac{\partial^2 u'}{\partial x'^2} + \frac{\partial^2 v'}{\partial y'^2}\right) + N\left(-u'B_y'^2 + v'B_x'B_y'\right),$$
$$u'\frac{\partial B_x'}{\partial x'} + v'\frac{\partial B_x'}{\partial y'} = \frac{1}{Re_m}\left(\frac{\partial^2 B_x'}{\partial x'^2} + \frac{\partial^2 B_x'}{\partial y'^2}\right). \tag{3}$$

Definition 1. *$Re = (\rho\, u_0 L)/\mu$ is called the Reynolds number and it represents the ratio of the internal forces to the viscous forces.*

Definition 2. *$Re_m = \mu\sigma L u_0$ is the magnetic Reynolds number.*

Definition 3. *$N = (\sigma L B_0)/(\rho\mu)$ is called the Stuart number and it represents the ratio of the electromagnetic forces to the internal forces.*

For simplification the prime symbol is omitted from the system of equations in (3).

Using a simplification of the Navier–Stokes and the magnetic-field-induction equations the fluid velocity as well as the magnetic field inside the channel, are calculated, by discretizing the domain and the equations with the finite volume method, creating a coupled system of non-linear algebraic equations which are solved using a Newton-like method.

In order to study the influence of the magnetic field on the fluid flow, the Lorentz force is introduced and applied to the fluid. The Lorentz force causes the velocity to drop. Using higher values of the Hartmann number, a stronger Lorentz force can be applied. The Lorentz force can be mathematically modelled using the term

$$\bar{f}_L = \bar{J} \times \bar{B}, \tag{4}$$

along with the Hartmann number, Ha, which is a non-dimensional number defined as

$$Ha = \sqrt{NRe}. \tag{5}$$

We assume that the electric current density $\bar{J}$, is equal to $\bar{q} \times \bar{B}$, resulting in

$$\bar{f}_L = (\bar{q} \times \bar{B}) \times \bar{B}, \tag{6}$$

which after the calculation of the outer products, the general case is $\bar{q} = (u, v, w)$ and $\bar{B} = (B_x, B_y, B_z)$, and more specifically in the two-dimensional case ($w = B_z = 0$) for the Lorentz force $\bar{f}_L$:

$$\bar{f}_L = \left(-uB_y^2 + vB_xB_y\right)\bar{i} + \left(uB_yB_x - vB_x^2\right)\bar{j} + 0\bar{k}. \tag{7}$$

It is assumed for the velocity that $v = 0$ and for the magnetic field $B_x = 0$ and $B_y = c$, giving for the Hartmann flow

$$\bar{f}_L = -uc^2\bar{i} + 0\bar{j} + 0\bar{k}. \tag{8}$$

In this formulation, it is assumed that the flow is laminar and the external magnetic field is constant in magnitude and vertical to the flow.

By calculating the norm of the Lorentz force, the effect of the force on the flow field is given by

$$\|\bar{f}_L\| = \sqrt{c^4 u^2} = c^2 |u|. \tag{9}$$

This implies that the relation of the Lorentz force and the fluid velocity is linear. A higher fluid velocity results in a higher magnitude of the Lorentz force. For the inducted magnetic field $\bar{B}$ and the Lorentz force $\bar{f}_L$ the following is concluded:

$$\bar{B} \perp \bar{f}_L. \tag{10}$$

The electric current I does not contribute in the two-dimensional case. Using the right-hand rule (the electric current does not contribute in the two-dimensional case) it can be seen that the Lorentz force retards the fluid velocity.

Remark 1. *Let us assume a parabolic profile in the inlet, no slip conditions on the walls, and Neumann conditions at the channel outlet. The Lorentz force will create thin boundary layers which, in this case, are called Hartmann layers, as well as a decrease in the fluid velocity, as the magnitude of the magnetic field increases. This will also be proven by the analytical solution provided in a later section where the greater the value of the Hartmann number is, the greater the drop of the velocity is.*

A straight channel is considered where an external magnetic field $\bar{B}$ is vertically applied, $\bar{B} = b\bar{j} = b(y,z)\bar{j}$. This parameter refers to the external magnetic field. The flow is driven by a uniform pressure gradient and the fluid flows vertically to the magnetic field, $\bar{q}$: $\bar{q} = u\bar{i} = u(y,z)\bar{i}$.

The magnetic field is composed of two factors, the external magnetic field and the magnetic field induced by the flow of the conducting fluid, resulting in

$$\bar{B} = \frac{Re_m}{Ha} b\bar{i} + 1\bar{j} = \left(\frac{Re_m}{Ha} b, 1 \right) = (B_x, B_y), \tag{11}$$

where we have scaled the induced part by the term Re_m/Ha. This equation refers to the induced magnetic field.

Substituting the results of Equation (11) into the steady-state induction equation, results in a time-independent magnetic field. It is also assumed that the flow is fully developed, implying $(\bar{q} \cdot \bar{\nabla}) \cdot \bar{B} = \bar{0}$, resulting in the x-component of the induction equation,

$$0 = \frac{1}{Re_m} \left(\frac{\partial^2 B_x}{\partial x^2} + \frac{\partial^2 B_x}{\partial y^2} \right) + \left(B_x \frac{\partial u}{\partial x} + B_y \frac{\partial u}{\partial y} \right) \tag{12}$$

and substituting Equation (11) into Equation (12) results in

$$\frac{1}{Ha} \frac{\partial^2 b}{\partial y^2} + \frac{\partial u}{\partial y} = 0 \Rightarrow \frac{\partial^2 b}{\partial y^2} + Ha \frac{\partial u}{\partial y} = 0. \tag{13}$$

For the electric current density $\bar{J}$ Ampere's law is used:

$$\bar{J} = \frac{1}{Re_m} (\bar{\nabla} \times \bar{B}). \tag{14}$$

Substituting Equation (11) into (14) results in

$$\bar{J} = \frac{1}{Re_m} \left(\frac{\partial}{\partial x}\bar{i} + \frac{\partial}{\partial y}\bar{j} + \frac{\partial}{\partial z}\bar{k} \right) \times \left(\frac{Re_m}{Ha} b\bar{i} + 1\bar{j} + 0\bar{k} \right) = \frac{1}{Ha} \left(0, \frac{\partial b}{\partial z}, -\frac{\partial b}{\partial y} \right), \tag{15}$$

resulting in the Lorentz force being expressed with the inducted term b.

Using Equation (15) with Equation (11), the Lorentz force is

$$\bar{J} \times \bar{B} = \frac{1}{Ha}\left(\frac{\partial b}{\partial y}, \ -\frac{Re_m}{Ha}b\frac{\partial b}{\partial y}, \ \frac{Re_m}{Ha}b\frac{\partial b}{\partial z}\right). \tag{16}$$

A fully developed flow is assumed, $(\bar{q}\cdot\bar{\nabla})\cdot\bar{q} = \bar{0}$, resulting in the x-momentum of the Navier–Stokes equation being

$$0 = -\frac{\partial p}{\partial x} + \frac{1}{Re}\left(\frac{\partial^2 u}{\partial y^2}\right) + \frac{Ha^2}{Re}\left(\frac{1}{Ha}\frac{\partial b}{\partial y}\right), \tag{17}$$

where for convenience it is assumed that $\partial p/\partial x = (-\rho\, u_0\, \mu)/(L^2\, \rho)$, and from the non-dimensional pressure (which is shown in the non-dimensionless Navier–Stokes) the following is concluded:

$$\frac{\partial p'}{\partial x'} = \frac{L}{\rho\, u_0^2}\frac{\partial p}{\partial x} = \frac{L}{\rho\, u_0^2}\left(-\frac{\rho\, u_0\, \mu}{L^2\, \rho}\right) = -\frac{\mu}{u_0\, L\, \rho} = -\frac{1}{Re}. \tag{18}$$

Substitution of Equation (18) into Equation (17) gives

$$0 = \frac{1}{Re} + \frac{1}{Re}\frac{\partial^2 u}{\partial y^2} + \frac{Ha^2}{Re}\frac{1}{Ha}\frac{\partial b}{\partial y} \Rightarrow \frac{\partial^2 u}{\partial y^2} + Ha\frac{\partial b}{\partial y} = -1. \tag{19}$$

Equations (13) and (19) describe the two-dimensional Hartmann flow, which will be discussed and studied in the next subsection.

2.2. Analytical Solution of the Hartmann Flow

In this subsection, the behaviour of an electrically conducting fluid is studied while an external magnetic field, constant in magnitude, is applied. In this case, it is assumed that the magnetic field is applied vertically to the flow, meaning that the magnetic field b is a function of the variable y or $b = b(y)$. A similar assumption can be considered for the u-velocity, $u = u(y)$. Along with many applications of this flow, this is a test problem due to the fact that, with a known analytical solution, the numerical solution obtained by the algorithm developed can be validated.

The system of PDEs that describe the Hartmann flow is

$$Ha\frac{\partial b}{\partial y} + \frac{\partial^2 u}{\partial y^2} = -1, \ \text{for } -1 < y < 1, \tag{20}$$

$$Ha\frac{\partial u}{\partial y} + \frac{\partial^2 b}{\partial y^2} = 0, \ \text{for } -1 < y < 1, \tag{21}$$

with the boundary conditions

$$u = 0, \quad \text{at} \quad y = \pm 1 \quad \text{and} \quad \pm\frac{\partial b}{\partial y} + \frac{1}{c}b = 0, \quad \text{at} \quad y = \pm 1, \tag{22}$$

which is a well-defined second-order, linear system with constant coefficients. Here, $c \to 0$ implies that the walls are electrically insulated.

The analytical solutions of Equations (20) and (21) that describe the Hartmann flow, with the boundary conditions (22) for the velocity u and the magnetic field b, are, respectively,

$$u(y) = \bar{u}\left(1 - \frac{\cosh(Hay)}{\cosh(Ha)}\right), \quad b(y) = -\frac{y}{Ha} + \bar{u}\frac{\sinh(Hay)}{\cosh(Ha)}, \tag{23}$$

where $\bar{u}$ is the characteristic magnitude of velocity:

$$\bar{u} = \frac{1}{Ha}\left(\frac{c+1}{c\,Ha + \tanh(Ha)}\right). \tag{24}$$

Since the analytical solution is known, various cases of Hartmann numbers can be studied. The cases of small and large values of the Hartmann number are examined. More specifically, the first case is as the Hartmann number approaches zero, $Ha \to 0$, and the second case is the Hartmann number being much greater than 1, $Ha \gg 1$.

The velocity profile of the Hartmann flow approaches asymptotically the parabolic profile of the hydrodynamic case for small values of the Hartmann number and high values of the Hartmann number create Hartmann layers and decrease the fluid velocity.

(i) ($Ha \to 0$) We substitute the Taylor expansion of the hyperbolic functions $\tanh(Ha)$ and $\cosh(Ha)$ as $Ha \to 0$ into Equation (24) and the analytical solution of the velocity, giving

$$\bar{u} = -\frac{3(1+c)}{Ha^2(-3-3c+Ha^2)} \quad \text{and} \quad u(y) = -\frac{3(1+c)(-1+y^2)}{(3+3c-Ha^2)(2+Ha^2)}. \tag{25}$$

respectively. Since we study the case of $Ha \to 0$ this implies that there is no magnetic field b; therefore, $b = 0$. By taking the limit,

$$\lim_{Ha \to 0} u(y) = \lim_{Ha \to 0} -\frac{3(1+c)(-1+y^2)}{(3+3c-Ha^2)(2+Ha^2)} = \frac{1}{2}\left(1-y^2\right), \tag{26}$$

it can be seen that the analytical solution of the velocity is similar to that of the hydrodynamic case (parabolic profile) as well as

$$\lim_{Ha \to 0} u(\pm 1) = \frac{1}{2}\left(1-(\pm 1)^2\right) = 0, \tag{27}$$

meaning that it satisfies the boundary conditions (22).

(ii) ($Ha \gg 1$) Substituting the exponential equivalent of the hyperbolic functions $\tanh(Ha)$ into Equation (24), as well as the hyperbolic functions $\cosh(Ha)$ and $\sinh(Ha)$ into the analytical solution for the velocity and the magnetic field. Since the case of large values of the Hartmann number is studied, the following relations

$$\bar{u} \to \frac{1}{Ha}\frac{c+1}{cHa+1} \Rightarrow \bar{u} \xrightarrow{Ha \gg 1} 0 \tag{28}$$

and

$$u(y) = \bar{u}\left(1-e^{Ha(y-1)}\right), \quad b(y) = -\frac{y}{Ha} + \bar{u}\left(e^{Ha(y-1)}\right), \quad |y| < 1, \tag{29}$$

hold true, for the characteristic magnitude of the velocity, and the analytical solutions of the velocity and the magnetic field, respectively. Equation (29) must satisfy the boundary conditions (22), where for the u-velocity we have

$$u(1) = \bar{u}\left(1-e^{Ha(1-1)}\right) = 0 \quad u(-1) = \bar{u}\left(1-e^{-2Ha}\right) \xrightarrow{Ha \gg 1} 0. \tag{30}$$

For the magnetic field, after some simplifications, the following relations

$$+b'(1) + \frac{1}{c}b(1) = 0, \quad -b'(-1) + \frac{1}{c}b(-1) = 0, \tag{31}$$

imply that the boundary conditions in (22) are satisfied for large Hartmann numbers.

From the asymptotic analytical solution of the velocity, an exponentially decreased profile is observed, where it maximizes in the core flow of the channel at $y = 0$ and is equal to

$$u_{max} = u(0) = \bar{u}\left(1 - e^{-Ha}\right) \xrightarrow{Ha \gg 1} 0. \tag{32}$$

This exponential velocity drop, according to [27], creates thin boundary layers close to the walls of the channel with an order of thickness, $\delta = \mathcal{O}\left(Ha^{-1}\right)$. We will further verify this statement by comparing the Hartmann layers in the numerical solution.

2.3. Ferrohydrodynamic Flow

In the previous flow, the main objective was to study the fluid flow in a channel under various circumstances, such as the application of a uniform, constant in magnitude, magnetic field vertical to the flow. The FHD case is a slightly different problem. In FHD, the magnetic field is generated from a source (point) outside or inside the flow.

Let us assume a three-dimensional model of a channel geometry. A wire is placed at the bottom at a distance α to the channel and at a distance β from the channel inlet. An electric current is applied to the wire which will create an axisymetric magnetic field. In a two-dimensional model, this implies that the wire, or in this case the source, has coordinates (α, β), as seen in Figure 1.
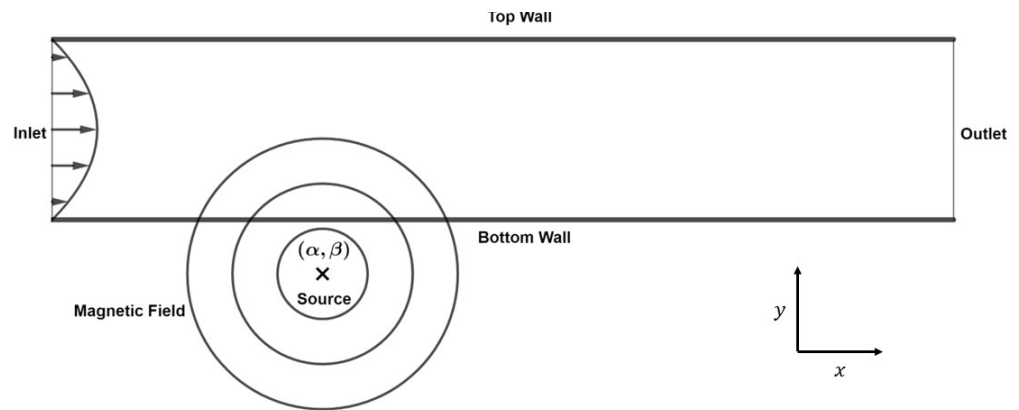

Figure 1. The source of the magnetic field (concentric circles with centre (α, β)) and the parabolic profile of the velocity at the inlet of the channel.

The distance at which the source is placed, as well as the magnitude of the magnetic field, will determine how much the parameters we study will change. The greater the distance of the source from the walls, the greater the magnitude of the magnetic field must be in order for the magnetic field to change the velocity and pressure profile.

The partial differential system of equations that formulate the FHD flow is

$$\rho\left(\frac{\partial u^2}{\partial x} + \frac{\partial uv}{\partial y}\right) = -\frac{\partial p}{\partial x} + \mu\left(\frac{\partial^2 u}{\partial x^2} + \frac{\partial^2 u}{\partial y^2}\right) + \mu_0 M \frac{\partial H}{\partial x},$$

$$\rho\left(\frac{\partial uv}{\partial x} + \frac{\partial v^2}{\partial y}\right) = -\frac{\partial p}{\partial y} + \mu\left(\frac{\partial^2 v}{\partial y^2} + \frac{\partial^2 v}{\partial y^2}\right) + \mu_0 M \frac{\partial H}{\partial y}, \tag{33}$$

$$\frac{\partial u}{\partial x} + \frac{\partial v}{\partial y} = 0$$

where ρ is the fluid density and μ is the fluid viscosity. The non-uniform magnetic field is formulated by new terms in the system of equations $\mu_0 M \bar{\nabla} H$, where M is a magnetization property which describes the behaviour of the fluid when it is exposed to a magnetic

field [5]. A linear equation for the isothermal case is, $M = \chi H$, where χ is a constant called the magnetic susceptibility [28] and is given as

$$H = H(x,y) = \sqrt{H_x^2 + H_y^2} = \frac{\gamma}{2\pi} \frac{1}{\sqrt{(x-\alpha)^2 + (y-\beta)^2}}, \tag{34}$$

where H is the magnitude of the magnetic field generated by the electric-current-carrying wire, and γ is the magnetic field strength at the current point.

The magnetic field in this flow is considered unaltered and depends only on the location of the source term. The Maxwell equations are not part of the FHD flow, rather the H was considered known and not influenced by the fluid flow. This assumption is used in the simulations presented.

The vector components of the magnetic field $\bar{H} = (H_x, H_y)$ are, respectively,

$$H_x(x,y) = -\frac{\gamma}{2\pi} \frac{x-\alpha}{(x-\alpha)^2 + (y-\beta)^2}, \quad H_y(x,y) = \frac{\gamma}{2\pi} \frac{y-\beta}{(x-\alpha)^2 + (y-\beta)^2}. \tag{35}$$

The objective is to study the non-dimensional equations from the governing system. The following non-dimensional parameters are introduced, and for the new terms the following formulation is used:

$$\bar{q}' = \frac{\bar{q}}{u_0}, \quad \bar{\nabla}' = L\bar{\nabla}, \quad p' = \frac{p}{\rho\, u_0^2}, \quad H' = \frac{H}{H_0}, \tag{36}$$

where $H_0 = H(\alpha, 0)$ is the magnitude of the magnetic field at the bottom wall. The dimensionless magnitude of the magnetic field is shown in Figure 2:

$$H' = \frac{H}{H_0} = \frac{\sqrt{H_x^2 + H_y^2}}{H_0} \Rightarrow$$
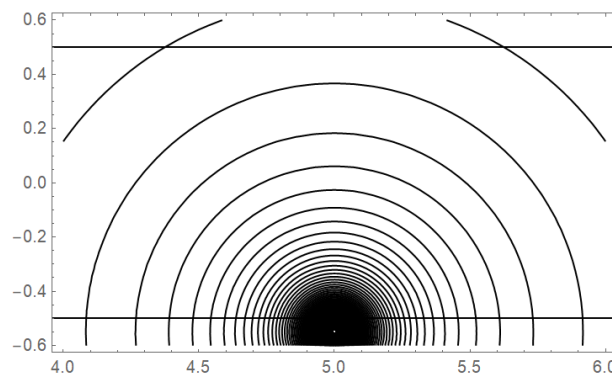$$H' = \frac{|\beta|}{\sqrt{(x-\alpha)^2 + (y-\beta)^2}}. \tag{37}$$

Figure 2. Contours of the dimensionless magnitude for the FHD flow with the wire placed at $(5, -0.55)$. The bottom wall is at $y = -0.5$ and the top wall is at $y = 0.5$.

The system of non-dimensional equations that formulate the FHD flow is along the conservation of mass, which remains the same:

$$(\bar{q}' \cdot \bar{\nabla}')\bar{q}' = -\bar{\nabla}'p' + \frac{1}{Re}\bar{\nabla}'^2\bar{q}' + Mn_F H'\bar{\nabla}'H'. \tag{38}$$

Definition 4. $Mn_F = (\mu_0 \chi H_0^2)/(\rho u_0^2)$ *is the **magnetic number for the FHD flow**.*

Expanding the vector form of Equation (38) into the equations in each momentum as follows while omitting the prime symbol for simplification:

$$\frac{\partial(u^2)}{\partial x} + \frac{\partial(uv)}{\partial y} = -\frac{\partial p}{\partial x} + \frac{1}{Re}\left(\frac{\partial^2 u}{\partial x^2} + \frac{\partial^2 u}{\partial y^2}\right) + Mn_F \frac{1}{2}\frac{\partial H^2}{\partial x},$$
$$\frac{\partial(uv)}{\partial x} + \frac{\partial(v^2)}{\partial y} = -\frac{\partial p}{\partial y} + \frac{1}{Re}\left(\frac{\partial^2 v}{\partial x^2} + \frac{\partial^2 v}{\partial y^2}\right) + Mn_F \frac{1}{2}\frac{\partial H^2}{\partial y}.$$
(39)

From a numerical perspective, the magnetization terms that enter the governing equations due to the principles of FHD constitute a "source term", which locally is of a greater order of magnitude than the other terms and gives rise to extended disturbances in the flow field, such as the formation of vortices. This could lead to a stiff numerical problem to solve. Thus, particularly for high values of the magnetic parameter combined with high-gradient magnetic fields, the calculation of the numerical solution is not a trivial task.

For the boundary conditions of the velocity, the parabolic profile is applied at the channel inlet and Neumann boundary conditions at the channel outlet. For the boundary conditions of the pressure, Neumann boundary conditions are applied at the channel inlet and at the channel outlet we assume zero pressure.

3. Numerical Solution

3.1. The Finite Volume Method on the Hartmann and FHD Flows

The discretized differential equations that describe the Hartmann flow are:
x-momentum

$$\frac{1}{2}Ha(b_N - b_S)\Delta x + (u_N - 2u_P + u_S)\frac{\Delta x}{\Delta y} + \Delta x\,\Delta y = 0,$$
(40)

x-induction

$$\frac{1}{2}Ha\,(u_N - u_S)\Delta x + (b_N - 2b_P + b_S)\frac{\Delta x}{\Delta y} = 0.$$
(41)

The discretized differential equations that describe the FHD flow are
x-momentum

$$\frac{1}{2}\left(u_E^2 - u_W^2\right)\Delta y + \frac{1}{2}(u_N v_N - u_S v_S)\Delta x = -(p_E - p_P)\Delta y +$$
$$+\frac{1}{Re}\left((u_E - 2u_P + u_W)\frac{\Delta y}{\Delta x}\right) + \frac{1}{Re}\left((u_N - 2u_P + u_S)\frac{\Delta x}{\Delta y}\right) + Mn_F\frac{1}{4}\left(H_E^2 - H_W^2\right)\Delta y,$$
(42)

y-momentum

$$\frac{1}{2}(u_E v_E - u_W v_W)\Delta y + \frac{1}{2}\left(v_N^2 - v_S^2\right)\Delta x = -(p_N - p_P)\Delta x +$$
$$+\frac{1}{Re}\left((v_E - 2v_P + v_W)\frac{\Delta y}{\Delta x}\right) + \frac{1}{Re}\left((v_N - 2v_P + v_S)\frac{\Delta x}{\Delta y}\right) + Mn_F\frac{1}{4}\left(H_N^2 - H_S^2\right)\Delta x.$$
(43)

Conservation of Mass

$$\frac{1}{2}(u_E - u_W)\Delta y + \frac{1}{2}(v_N - v_S)\Delta x = 0,$$
(44)

Remark 2. *These equations of differences, Equations (40) and (41) for the Hartmann flow as well as Equations (42)–(44) for the FHD flow, hold for all finite volume cells in the computational domain. For example, if we have a 10×10 computational grid, the equations of differences for this domain will be $100 \times 3 = 300$ algebraic equations.*

3.2. Numerical Method

For the numerical results and the simulations a CFD algorithm (a definition of which can be found in [26]) was created for the numerical solution of the Navier–Stokes equations. The numerical solution is obtained using a direct approach, which creates more robust results since the governing equations of each problem are altered as little as possible.

In order to obtain the numerical solution, we create the mesh in the domain studied, creating volumes. The FVM is applied to the governing equations, transforming them from non-linear PDEs into a system of coupled non-linear AEs. The unknowns are the values of the u- and v-velocities as well as the pressure p at each control volume of the mesh grid. The numerical solution of the coupled system is obtained utilizing a non-linear solver (Newton's method). The flow chart in Figure 3 depicts the algorithm steps used. $\bar{x}^n$ is the vector of the unknown variables created by the mesh grid and $\bar{f}(\bar{x}^n)$ is the coupled algebraic functions (system) evaluated at $\bar{x}^n$. The boundary conditions are given at the channel inlet and outlet and at the top and bottom walls, respectively. In the FVM, the partition of each direction of the control volumes is shown below:

$$
\begin{aligned}
u_E &= u(i+1,j), \ u_W = u(i-1,j), \ u_S = u(i,j-1), \ u_N = u(i,j+1), \\
v_E &= v(i+1,j), \ v_W = v(i-1,j), \ v_S = v(i,j-1), \ v_N = v(i,j+1), \\
p_E &= p(i+1,j), \ p_W = p(i-1,j), \ p_S = p(i,j-1), \ p_N = p(i,j+1), \\
u_P &= u(i,j), \quad v_P = v(i,j), \quad p_P = p(i,j)
\end{aligned}
\tag{45}
$$

where $i = 1, \ldots, N_x$ and $j = 1, \ldots, N_y$. Assuming that we use a grid of $N_x \times N_y$, this implies that there are $N_x N_y$ of each variable of Equation (45).

The algebraic system is given by evaluating each of the discretized equations in each control volume of the partition. For example, the evaluation of the x-momentum of the FHD fluid flow in each control volume of the grid creates the first $N_x N_y$ equations for the algebraic system, the evaluation of the y-momentum results in the creation of the next $N_x N_y$ equations, and finally the evaluation of the continuity gives the rest of the $N_x N_y$ equations. In total, the system has $3 N_x N_y$ algebraic equations.

In summary, the system of algebraic equations for the FHD fluid flow is, $\bar{f} = (F_1, F_2, F_3)$, with F_1 equal to Equation (42), F_2 equal to Equation (43), and F_3 equal to Equation (44), using the formulation in (45). A similar methodology is used for the equations of the Hartmann fluid flow. Finally, the Jacobian matrix is given by

$$
\bar{J} = \begin{pmatrix}
(F_1)_u & (F_1)_v & (F_1)_p \\
(F_2)_u & (F_2)_v & (F_2)_p \\
(F_3)_u & (F_3)_v & (F_3)_p
\end{pmatrix}
\tag{46}
$$

After the convergence of the algorithm, the output is the values of the velocities u and v and the pressure p at each control volume of the partition. In summary, the whole domain's equations (three equations for each control volume) are solved simultaneously at each iteration of the Newton's algorithm. So, the iterations depicted in Figure 3 of the CFD algorithm lead to the convergence of the numerical scheme.

The finite volume method, a second-order accuracy method, due to the central differences used for the discretization of the governing equations, transforms the governing non-linear system of partial differential equations (conservation of mass and Navier–Stokes) into a highly non-linear and tightly coupled system of algebraic equations with intense source terms, such as the non-uniform magnetic field. Firstly, the method discretizes the domain into smaller, finite in number, domains (resulting in the creation of a grid), as can be seen in Figure 4a. The unknown variables are calculated on the grid points, which can be seen in Figure 4b.
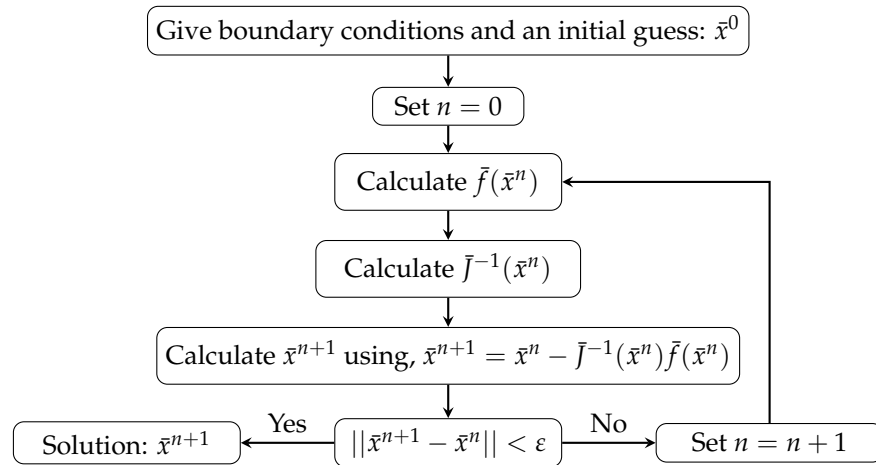
Figure 3. Flowchart of the CFD algorithm. The coupled system $\bar{f}(\bar{x}^n) = \bar{0}$ is solved simultaneously at each Newton iteration.
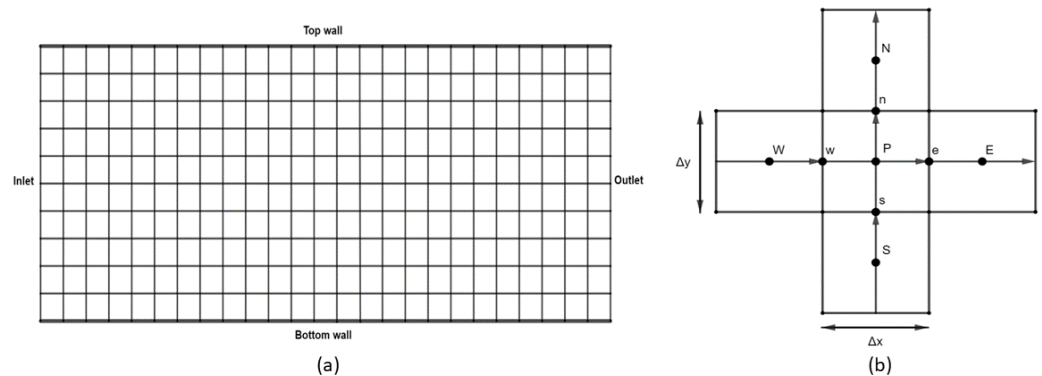

Figure 4. (**a**) The grid created in the channel and (**b**) the grid created in the channel.

In the FVM, the terms in the conservation equation represent the face fluxes and are evaluated at the finite volume faces w, e, p, n, and s. Because the values at these faces are not known, a numerical approach is used whereby the mean values based on the neighbouring grid points W, E, P, N, and S are calculated. Because the flux entering a given volume is similar to that leaving the adjacent volume, the FVM is conservative or divergence free, i.e., $\bar{\nabla} \cdot \bar{q} = 0$. Finally, in the FVM, it is easy to implement a variety of boundary conditions in a non-invasive manner, since the unknown variables are evaluated at the centroids of the volume elements not at the boundary faces [26].

3.3. Direct Solution Approach

In the field of fluid dynamics, the fluid flows are described by a set of governing equations in which the dominant variables are present in other ones as well, e.g., conservation of mass and Navier–Stokes equations. In the simultaneous approach which is used in this study, all equations compose a single system of equations which is discretized using the finite volume method. This approach on a very fine grid can be very time consuming and expensive in terms of memory when the system is non-linear and tightly coupled. The numerical solution for the case of Hartmann flow is less expensive since the equations that describe this flow are simplified to a linear system of equations. This statement is not true for the case of the FHD flow. The equations are not simplified and create a non-linear coupled system, and due to the magnetic field source term being a non-linear system, as the magnitude increases the method is very expensive in order to converge. Despite this disadvantage this method produces a very good solution. The Hartmann flow has been studied for the grid sizes of $10 \times 10, 20 \times 20, 40 \times 40, 80 \times 80$, and 160×160. The FHD flow has been examined for grid sizes of $350 \times 35, 400 \times 40, 450 \times 45$, and 500×50.

In order to find a numerical solution to the Navier–Stokes equations, various techniques, e.g., pressure correction algorithms or linearization approaches, have been developed by several researchers such as Patankar [29]. These methods assume a solution at first, which is then substituted into the equations and corrected through algorithm steps. The numerical solution is obtained using a direct approach, which creates more robust results since the governing equations of each problem are altered as little as possible. An initial guess is used for the algorithm steps to begin.

Another approach for the numerical solution of the system under consideration is the usage of iterative methods such as those of Shyy [30] and Patankar [29]. In such methods, the unknown variables are evaluated at the control volume faces and are corrected, and thus updated, until the new value is as close to the previous correction as the user needs. This results in methods with lower computational and time costs, but lacking in robustness compared to the direct method [31].

4. Results and Discussion

4.1. Numerical Results for the Hartmann Flow

The solution of the algebraic system of the Hartmann flow is validated in this subsection. In Table 1, using as a gold standard the analytical solutions in the inlet, the results of comparing the analytical to the numerical solution at the channel outlet are observed.

The root mean square (RMS)

$$RMS = \sqrt{\frac{1}{N}\sum_{i=1}^{N}|\bar{x}_i - x_i^2|}, \tag{47}$$

measures the difference of the numerical solution, $\bar{x}_i$, with the analytical one, x_i. The parameter N is the size of the data, or in this case, the nodes of the partition. The RMS values shown in Table 1 indicate that the analytical solution for the velocity and the induced magnetic field of the Hartmann flow are very close, thus validating the results.

In Figure 5, a reduction in the velocity profile inside the channel is observed as the Hartmann number is increased, implying a stronger magnetic field. In the hydrodynamic case, the maximum velocity is $u_{max} = 0.5$. Due to the Lorentz forces the maximum value drops, taking values of $u_{max} \approx 0.48, 0.37, 0.25, 0.17, 0.12$, and 0.1 for $Ha = 1, 2, 4, 6, 8$, and 10, respectively.
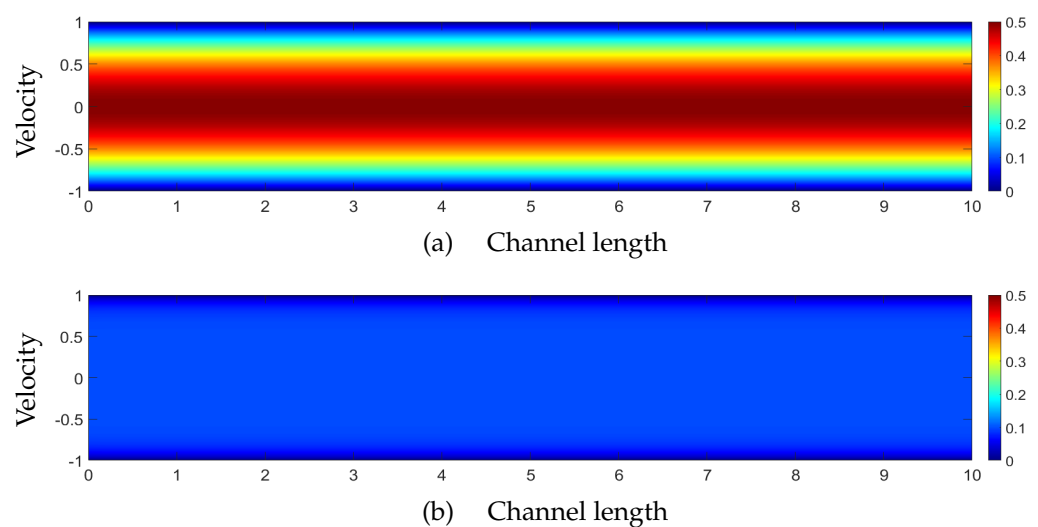

Figure 5. Contour plots of the velocity for (**a**) $Ha = 0$ (Hydrodynamic case) and (**b**) $Ha = 10$ for the Hartmann flow.

Table 1. Difference (error) between the analytical and the numerical solution of the velocity and the induced magnetic field, for the Hartmann flow, using the root mean square formulation, for various grid sizes and different cases of the Hartmann number, $Ha = 1, 2, 4, 6, 8$, and 10.

	RMS Velocity		**RMS Magnetic Field**	
Grid	$Ha = 1$	$Ha = 2$	$Ha = 1$	$Ha = 2$
10×10	8.6524×10^{-4}	2.1329×10^{-3}	2.2090×10^{-4}	1.1121×10^{-3}
20×20	2.3122×10^{-4}	5.6631×10^{-4}	5.9014×10^{-5}	2.9440×10^{-4}
40×40	5.9878×10^{-5}	1.4639×10^{-4}	1.5279×10^{-5}	7.6020×10^{-5}
80×80	1.5244×10^{-5}	3.7250×10^{-5}	3.8896×10^{-6}	1.9338×10^{-5}
160×160	3.8463×10^{-6}	9.3976×10^{-6}	9.8138×10^{-7}	4.8784×10^{-6}
Grid	$Ha = 4$	$Ha = 6$	$Ha = 4$	$Ha = 6$
10×10	3.1142×10^{-3}	3.8286×10^{-3}	2.8555×10^{-3}	3.8122×10^{-3}
20×20	8.1345×10^{-4}	9.7631×10^{-4}	7.4144×10^{-4}	9.7069×10^{-4}
40×40	2.0911×10^{-4}	2.4841×10^{-4}	1.9024×10^{-4}	2.4685×10^{-4}
80×80	5.3129×10^{-5}	6.2919×10^{-5}	4.8308×10^{-5}	6.2515×10^{-5}
160×160	1.3396×10^{-5}	1.5854×10^{-5}	1.2181×10^{-5}	1.5752×10^{-5}
Grid	$Ha = 8$	$Ha = 10$	$Ha = 8$	$Ha = 10$
10×10	4.5678×10^{-3}	5.2448×10^{-3}	4.5674×10^{-3}	5.2448×10^{-3}
20×20	1.1441×10^{-3}	1.3037×10^{-3}	1.1438×10^{-3}	1.3037×10^{-3}
40×40	2.8760×10^{-4}	3.2367×10^{-4}	2.8752×10^{-4}	3.2367×10^{-4}
80×80	7.2552×10^{-5}	8.1256×10^{-5}	7.2531×10^{-5}	8.1255×10^{-5}
160×160	1.8261×10^{-5}	2.0424×10^{-5}	1.8256×10^{-5}	2.0424×10^{-5}

The Hartmann layers are more and more visible as the magnitude of the magnetic field increases, as shown in Figure 6. The parameter $\delta = \mathcal{O}(Ha^{-1})$ refers to the thickness of the Hartmann boundary layers created by the drop in the velocity due to the Lorentz force. This implies that their thicknesses are $\delta \approx 1/Ha$ for each Hartmann number.
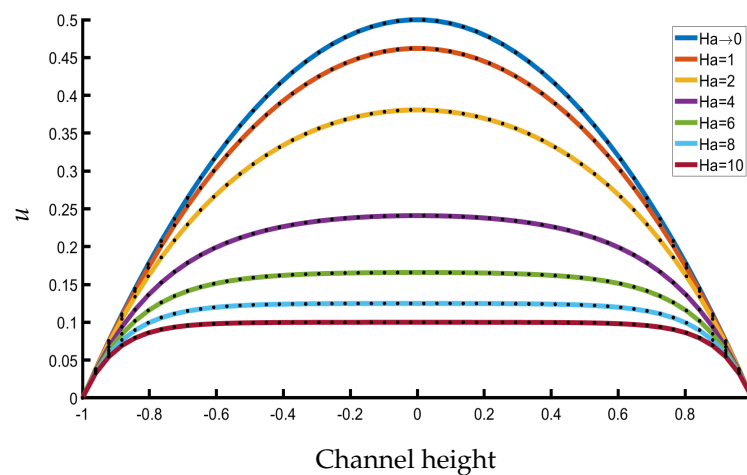

Figure 6. The velocity profiles of the Hartmann flow for different values of the Hartmann number. The black dots represent the analytical velocity for each value of the Hartmann number.

The hydrodynamic case ($Ha = 0$) implies that there is no magnetic field. In Figure 7, the behaviour of the magnetic field inside the channel is shown, which can be explained

due to the boundary conditions (22), the insulating walls, and the conducting fluid. Zero magnetic field is assumed at the channel inlet and outlet, respectively.
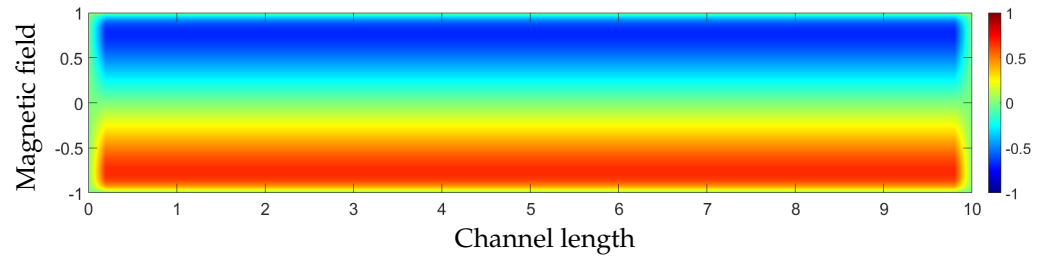

Figure 7. Contour plot of the magnetic field for $Ha = 10$ for the Hartmann flow.

The increase in the Hartmann number creates a steeper profile of the magnetic field, as shown in Figure 8.
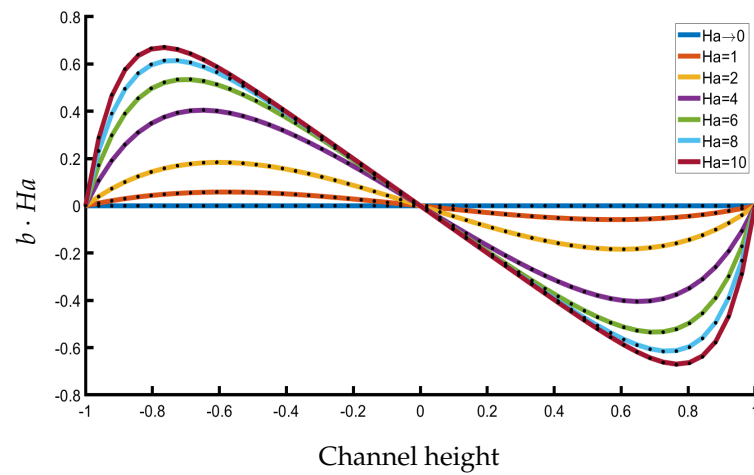

Figure 8. The magnetic field profiles of the Hartmann flow for different values of the Hartmann number, multiplied by the respective Hartmann number (bHa). The black dots represent the analytical velocity for each value of the Hartmann number.

4.2. Numerical Results for the Ferrohydrodynamic Flow

While the flow is disturbed at the magnetic source point, the flow becomes fully developed further away from the source. This can be seen in Figure 9, which depicts the case of the stronger magnetic field studied by the authors.
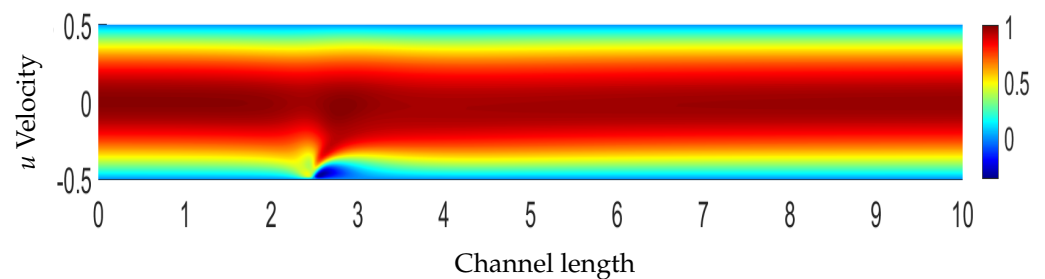
Figure 9. Contour plot of the u-velocity for $Mn_F = -0.4$ for the FHD flow.

In Table 2, the percentage difference between various grid sizes is depicted. The unknown parameters have been examined locally, close to the vortex created (point of interest) by the FHD theory. Along with the percentage difference, the number of equations solved for each grid case is depicted. A relatively small change in the grid size can create a larger coupled system of equations than the solver is able to solve.

Table 2. Number of equations solved simultaneously and percentage difference between grids for the parameters studied at $x = 2.62$ and for $Mn_F = -0.4$. The difference becomes smaller as the grid becomes finer.

Grid	Equations	% Difference between Grids		
		$u(2.62, y)$	$v(2.62, y)$	$p(2.62, y)$
224×59	39,648	2.4896	2.7152	2.3424
224×79	53,088	1.2088	1.3117	1.3627
224×99	66,528	0.7056	0.8986	0.7942
224×119	79,968	—	—	—

Figure 10 shows the local distribution of the u-velocity component at $x = 2.62$ or $u(2.62, y)$ for $Mn_F = -0.4$, which creates the most disturbance inside the field flow. As the grid becomes finer, the distributions are closer to each other. The u-velocity takes negative values, indicating the recirculation of the fluid flow.
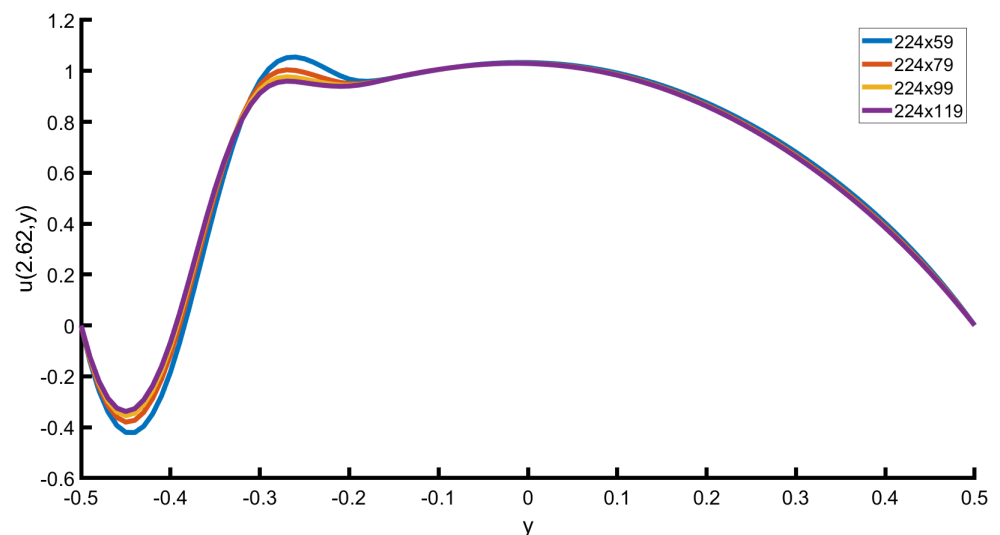
Figure 10. Distribution of the u-velocity for the case of $Mn_F = -0.4$ at $x = 2.62$, for various grid sizes.

In Figure 11, the local, steep drop of pressure is presented, which is at the position of the magnetic source. Higher magnitudes result in steeper drops. This can be explained by the flow recirculation (creation of vortices), implying that the fluid flows in the opposite direction. The creation of vortices can also be seen in [5,10,28]. The maximum value at the channel inlet reduces as the magnitude rises, representing a local stenosis.

The vortices are present even at lower magnitude (Figures 12–15) due to the close distance of the wire. For magnitudes of 0.7, 0.85, and 1.0, the maximum value of the flow remains the same as the hydrodynamic case, whereas for 1.15 a slight increase in it is observed. Figures 12–15 depict the creation of the vortex using the stream lines (white ones). These figures show a magnification near the magnetic field source. As the magnetic field source is placed further away from the bottom plate, more intense magnetic fields are needed for the creation of vortices. As the source is placed closer to the wall, a smaller magnetic field magnitude is needed for the creation of a vortex. The authors decided not to include these cases due to space economy, but the case of a fixed position magnetic field source is presented.
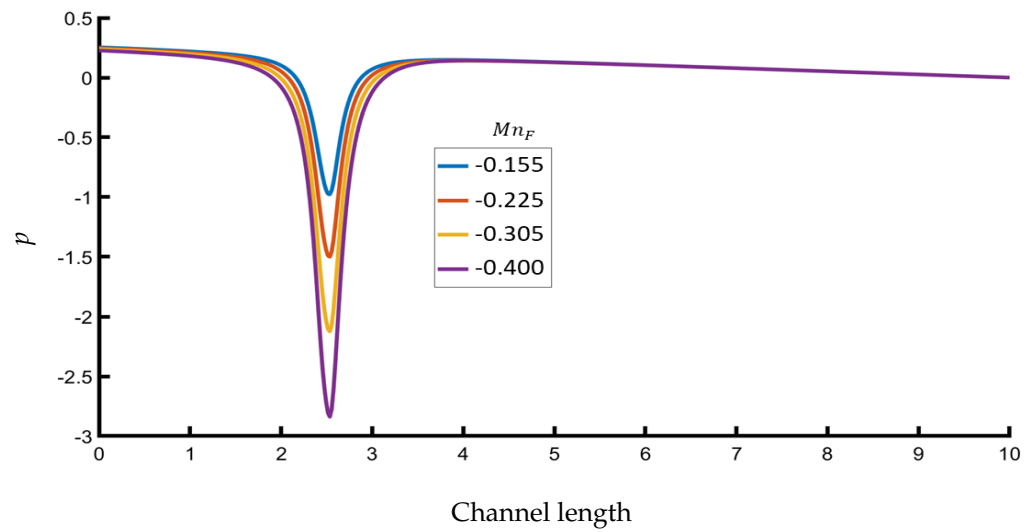
Figure 11. The profile of the pressure for a fluid particle close to the bottom channel wall.
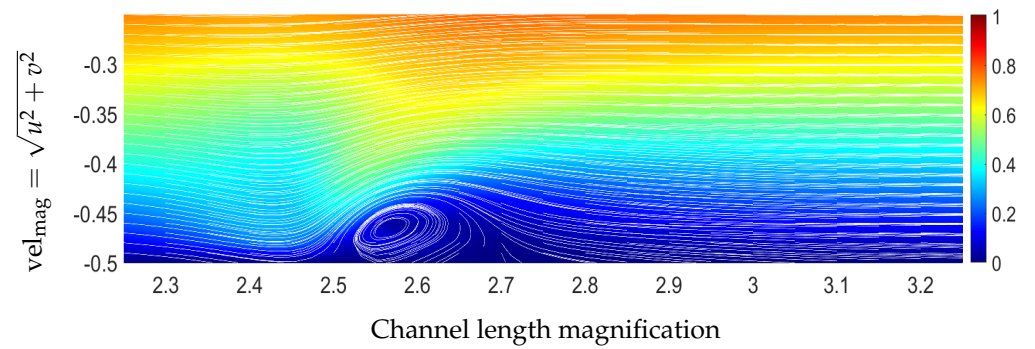

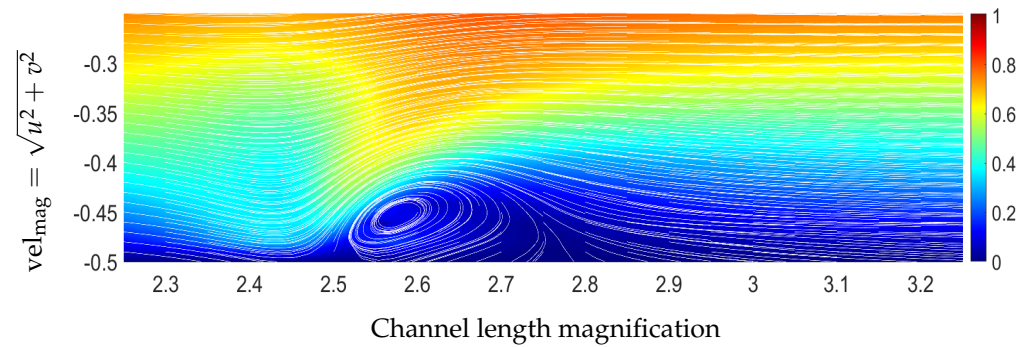**Figure 12.** Vortex created for $Mn_F = -0.155$ near the bottom wall of the channel.

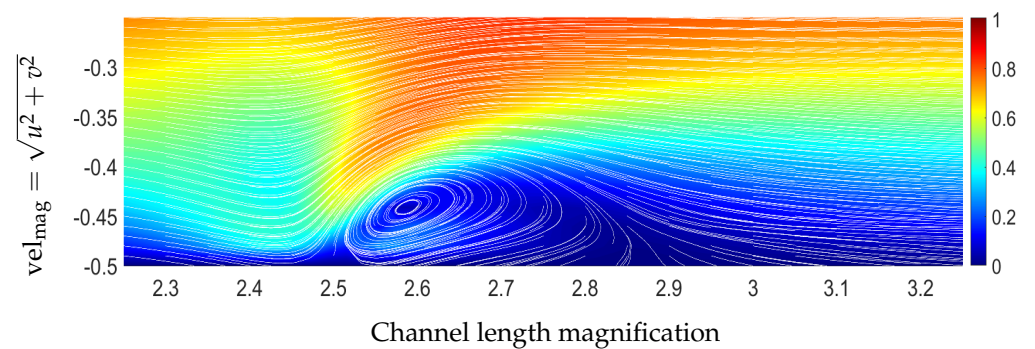**Figure 13.** Vortex created for $Mn_F = -0.225$ near the bottom wall of the channel.

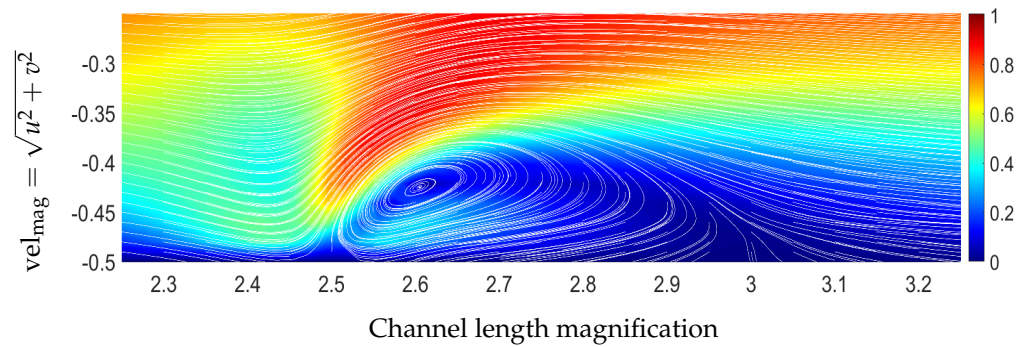**Figure 14.** Vortex created for $Mn_F = -0.305$ near the bottom wall of the channel.

Figure 15. Vortex created for $Mn_F = -0.400$ near the bottom wall of the channel.

In summary, the Hartmann flow is described by the x-momentum of the Navier–Stokes and the magnetic-field-induction equations, respectively. The FHD flow is described by the conservation of mass and the x- and y-momentums of the Navier–Stokes equations, assuming that the magnetic field is always the same and not altered by the flow. Although the induced magnetic field equation can be implemented in the FHD flow, it is not considered in this study at all.

The induced magnetic field equation is part of the system in the Hartmann flow, and with some simplifications the analytical solution of it can be found, as shown in Equation (23). In the case of the FHD flow, the induced magnetic field equations are not part of the system of equations, assuming that the magnetic field is always the same, and is dependent on the spatial parameters only, as shown in Equation (34); hence, there is no analytical or numerical solution for it in this study.

4.3. Non-Dimensional Numbers

For the problems introduced in this study, specific values for the non-dimensional numbers

$$Re = \frac{\rho u_0 L}{\mu}, \quad N = \frac{\sigma L B_0}{\rho \mu}, \quad Mn_F = \frac{\mu_0 \chi H_0^2}{\rho u_0^2}, \quad \bar{\nabla}' = L \bar{\nabla}. \tag{48}$$

are applied.

In order to assign values to the dimensionless numbers above, a realistic case will be studied, which is blood flow in a channel [10]. For this case the density is $\rho = 1050 \, \text{kg m}^{-3}$, dynamic viscosity is $\mu = 3.2 \cdot 10^{-3} \, \text{kg m}^{-1} \, \text{s}^{-1}$, the characteristic velocity is $u_0 = 4.0 \cdot 10^{-2} \, \text{m s}^{-1}$, and the characteristic length of the channel is $L = 0.022 \, \text{m}$ due to the parabolic profile at the inlet. The electrical conductivity for the blood is $\sigma = 0.8 \, \text{S/m}$ and the magnetic field magnitude can be expressed as $B_0 = \mu_0 H_0$. The magnetic permeability of the vacuum is $\mu_0 = 4\pi \cdot 10^{-7} \, \text{N/A}^2$ and the magnetic susceptibility is $\chi = -6.6 \cdot 10^{-7}$.

Substituting the values into Equation (48) gives $Re \approx 300$. For the Hartmann flow, the parameter that changes the behaviour of the fluid flow significantly is the Hartmann number, where we choose constant values, including the values of the Reynolds and Stuart numbers inside that constant. For the values of the non-dimensional number Mn_F the values above are applied and different magnetic field magnitudes are used depending on the problem under consideration.

4.4. Conclusions

Hartmann flow: The Hartmann flow describes the flow of an electrically conducting fluid between two parallel-plate walls as an external induced magnetic field is vertically applied to the channel's bottom wall. The application of the magnetic field results in an increase in the fluid drag due to the Lorentz force opposing the fluid flow. The drop in velocity results in the creation of the Hartmann layers. The magnetic field in the channel is also studied, where, due to the electrically conducting fluid, it is affected. Applying simplifications to the governing equations results in the analytical solution for

the velocity as well as the magnetic field in the channel. The numerical solutions match the analytical ones very well, introducing another test problem for the validation of the numerical procedure.

FHD flow: FHD is a fluid flow based on FHD principles, which describes a fluid flow with enhanced fluid conductivity so that it can be affected by an external magnetic field point source, constant in magnitude. The source is an electrically conducting wire placed close to the bottom wall with a fixed position of $(2.5, -0.6)$. By applying an electrical current through the wire, a symmetrical magnetic field is created, affecting the fluid in the channel. The results are the creation of a main vortex near the magnetic field source, changing the direction of the fluid by the recirculation of the flow close to the magnetic source. The pressure near the source is drastically decreased, explaining the creation of the vortex. These pressure changes are similar to the stenosis case of a channel. These results are the same as previously published studies [10].

Abbreviations

The following abbreviations are used in this manuscript:

AE	Algebraic equation
PDE	Partial differential equation
FVM	Finite volume method
FEM	Finite element method
MPCM	Meshless point collocation method
MLS	Moving least squares
MHD	Magnetohydrodynamic
FHD	Ferrohydrodynamic
BFD	Biomagnetic fluid dynamics
CFD	Computational fluid dynamics

References

1. Elelamy, A.F. Laser Effects on Bioheat Transfer with Non-Newtonian Hybird Nanofluid Flow: Analytical Method with Finite Sine and Laplace Transforms. *J. Nanofluids* **2023**, *12*, 1224–1232. [CrossRef]
2. Shamshuddin, M.; Asogwa, K.K.; Ferdows, M. Thermo-solutal migrating heat producing and radiative Casson nanofluid flow via bidirectional stretching surface in the presence of bilateral reactions. *Numer. Heat Transf. Part Appl.* **2023**, 1–20. [CrossRef]
3. Bozkır, S.C.; Çobanoğlu, N.; Doğanay, S.; Karadeniz, Z.H.; Elçioğlu, E.B.; Turgut, A. Investigation of External Magnetic Field Effect on The Performance of Ferrofluid-based Single-Phase Natural Circulation Loops. *Therm. Sci. Eng. Prog.* **2023**, *42*, 101921. [CrossRef]
4. Kai, Y.; Ahmad, S.; Takana, H.; Ali, K.; Jamshed, W.; Eid, M.R.; Abd-Elmonem, A.; El Din, S.M. Thermal case study and generated vortices by dipole magnetic field in hybridized nanofluid flowing: Alternating direction implicit solution. *Results Phys.* **2023**, *49*, 106464. [CrossRef]
5. Tzirtzilakis, E. A mathematical model for blood flow in magnetic field. *Phys. Fluids* **2005**, *17*, 077103. [CrossRef]
6. Kumar, D.; Subudhi, S. Buoyancy induced convection in magnetite nanofluid filled in enclosure with thick fin under magnetic field produced by a magnetic source. *J. Magn. Magn. Mater.* **2023**, *575*, 170725. [CrossRef]

7. Haik, Y.; Pai, V.; Chen, C.J. Development of magnetic device for cell separation. *J. Magn. Magn. Mater.* **1999**, *194*, 254–261. [CrossRef]

8. Davidson, P.A. *Introduction to Magnetohydrodynamics*, 2nd ed.; Cambridge Texts in Applied Mathematics; Cambridge University Press: Cambridge, UK, 2016. [CrossRef]

9. Siddiqa, S.; Naqvi, S.; Begum, N.; Awan, S.; Hossain, M. Thermal radiation therapy of biomagnetic fluid flow in the presence of localized magnetic field. *Int. J. Therm. Sci.* **2018**, *132*, 457–465. [CrossRef]

10. Loukopoulos, V.; Tzirtzilakis, E. Biomagnetic channel flow in spatially varying magnetic field. *Int. J. Eng. Sci.* **2004**, *42*, 571–590. [CrossRef]

11. Benal, S.S.; Tawade, J.V.; Biradar, M.M.; Allasi, H.L.; Ashraf, M.W. Effects of the Magnetohydrodynamic Flow within the Boundary Layer of a Jeffery Fluid in a Porous Medium over a Shrinking/Stretching Sheet. *Math. Probl. Eng.* **2022**, *2022*, 7326504. [CrossRef]

12. Punith Gowda, R.; Naveen Kumar, R.; Prasannakumara, B.; Nagaraja, B.; Gireesha, B. Exploring magnetic dipole contribution on ferromagnetic nanofluid flow over a stretching sheet: An application of Stefan blowing. *J. Mol. Liq.* **2021**, *335*, 116215. [CrossRef]

13. Zhao, T.H.; Khan, M.I.; Qayyum, S.; Kumar, R.N.; Chu, Y.M.; Prasannakumara, B.C. Comparative study of ferromagnetic hybrid (manganese zinc ferrite, nickle zinc ferrite) nanofluids with velocity slip and convective conditions. *Phys. Scr.* **2021**, *96*, 075203. [CrossRef]

14. Guled, C.; Tawade, J.; Kumam, P.; Noeiaghdam, S.; Maharudrappa, I.; Chithra, S.; Govindan, V. The heat transfer effects of MHD slip flow with suction and injection and radiation over a shrinking sheet by optimal homotopy analysis method. *Results Eng.* **2023**, *18*, 101173. [CrossRef]

15. Mahesh, R.; Mahabaleshwar, U.; Kumar, P.V.; Öztop, H.F.; Abu-Hamdeh, N. Impact of radiation on the MHD couple stress hybrid nanofluid flow over a porous sheet with viscous dissipation. *Results Eng.* **2023**, *17*, 100905. [CrossRef]

16. Türk, Ö.; Bozkaya, C.; Tezer-Sezgin, M. A FEM approach to biomagnetic fluid flow in multiple stenosed channels. *Comput. Fluids* **2014**, *97*, 40–51. [CrossRef]

17. Türk, Ö.; Tezer-Sezgin, M.; Bozkaya, C. Finite element study of biomagnetic fluid flow in a symmetrically stenosed channel. *J. Comput. Appl. Math.* **2014**, *259*, 760–770. [CrossRef]

18. Bhargava, R.; Bég, O.A.; Sharma, S.; Zueco, J. Finite element study of nonlinear two-dimensional deoxygenated biomagnetic micropolar flow. *Commun. Nonlinear Sci. Numer. Simul.* **2010**, *15*, 1210–1223. [CrossRef]

19. Tezcan, M.M.; Yetgin, A.G.; Canakoglu, A.I.; Cevher, B.; Turan, M.; Ayaz, M. Investigation of the effects of the equivalent circuit parameters on induction motor torque using three different equivalent circuit models. *MATEC Web Conf.* **2018**, *157*, 01019. [CrossRef]

20. Sheikholeslami, M.; Hayat, T.; Alsaedi, A. Numerical study for external magnetic source influence on water based nanofluid convective heat transfer. *Int. J. Heat Mass Transf.* **2017**, *106*, 745–755. [CrossRef]

21. Tezer-Sezgin, M.; Bozkaya, C.; Türk, Ö. BEM and FEM based numerical simulations for biomagnetic fluid flow. *Eng. Anal. Bound. Elem.* **2013**, *37*, 1127–1135. [CrossRef]

22. Ayob, A.R.C.; Ismail, Z.; Kasiman, E.H. Least-Squares Finite Element Method for Solving Stokes Flow under Point Source Magnetic Field. *Symmetry* **2022**, *14*, 514. [CrossRef]

23. Strek, T.; Jopek, H. Computer simulation of heat transfer through a ferrofluid. *Phys. Status Solidi* **2007**, *244*, 1027–1037. [CrossRef]

24. Boutopoulos, I.D.; Lampropoulos, D.S.; Bourantas, G.C.; Miller, K.; Loukopoulos, V.C. Two-phase biofluid flow model for magnetic drug targeting. *Symmetry* **2020**, *12*, 1083. [CrossRef]

25. Loukopoulos, V.; Bourantas, G.; Labropoulos, D.; Nikiforidis, V.; Bordas, S.P.; Nikiforidis, G. Numerical study of magnetic particles concentration in biofluid (blood) under the influence of high gradient magnetic field in microchannel. In Proceedings of the 7th European Congress on Computational Methods in Applied Sciences and Engineering: ECCOMAS Congress, Crete Island, Greece, 5–10 June 2016; National Technical University of Athens: Athens, Greece, 2016; pp. 1084–1092.

26. Darwish, M.; Moukalled, F. *The Finite Volume Method in Computational Fluid Dynamics: An Advanced Introduction with OpenFOAM®️ and Matlab®️*; Springer: Berlin/Heidelberg, Germany, 2016.

27. Müller, U.; Bühler, L. *Magnetofluiddynamics in Channels and Containers*; Springer Science & Business Media: Berlin/Heidelberg, Germany, 2013.

28. Tzirtzilakis, E.; Xenos, M. Biomagnetic fluid flow in a driven cavity. *Meccanica* **2013**, *48*, 187–200. [CrossRef]

29. Patankar, S. *Numerical Heat Transfer and Fluid Flow*; Electro Skills Series; Hemisphere Publishing Corporation: New York, NY, USA, 1980.

30. Shyy, W.; Udaykumar, H.; Rao, M.M.; Smith, R.W. *Computational Fluid Dynamics with Moving Boundaries*; Courier Corporation: North Chelmsford, MA, USA, 2012.

31. Xenos, M. An Euler–Lagrange approach for studying blood flow in an aneurysmal geometry. *Proc. R. Soc. A Math. Phys. Eng. Sci.* **2017**, *473*, 20160774. [CrossRef]